Effect of Surface Passivation on $Cd_xNi_{1-x}S$ Thin Films Embedded with Nickel Nanoparticles

Cliff Orori Mosiori [1]

[1] *Technical University of Mombasa*
P. O. Box 90420-80100, Mombasa, Kenya

DOI: 10.22178/pos.25-4

LCC Subject Category: TP155-156, QC450-467, QD450-801

Received 12.06.2017
Accepted 10.08.2017
Published online 16.08.2017

Corresponding Author:
corori@tum.ac.ke

Abstract. Certain treatments done to binary *CdS*, such as incorporating *Ni* onto *CdS* produces ternary thin films may cause major optical parameters that have a number of applications including for solar cell device fabrication. In this paper, we report on the effect of surface passivation on the band gap and other related optical properties of *CdNiS* thin films. Thin films for $Cd_xNi_{1-x}S$ were prepared on glass substrates by chemical solution method. Effects of surface passivation and variation of the volume of nickel ions on the optical properties *CdS* hence obtaining $Cd_xNi_{1-x}S$ thin films was investigated. It was observed that the thin films hard an average Transmittance above 68 %, with *reflectance* below 25 % across UV-VIS-NIR region. A plot of $(ahv)^2$ versus *hv* gave energy band gap between 2.55–3.49 eV for as-grown samples and 2.82–3.50 eV for annealed samples. The passivated samples had *band gap* energy values within the range 2.85–3.12 eV. It was concluded that an increase in concentration of Cd^{2+} and Ni^{2+} ions in the reaction led to an increase the *band gap* while *optical conductivity* ranged between 3.78×10^{11}–2.40×10^{12} S^{-1}.

Keywords: absorbance; annealing; optical conductivity; solar cell; spectrophotometer.

INTRODUCTION

Certain treatments done to binary *CdS*, such as incorporating *Ni* onto *CdS* produces ternary thin films. Such ternary thin film materials may cause major change in the optical parameters that may have a number of optoelectronic applications. It may have a direct influence on the electrical properties of the resulting material or the modification may result into some properties useful for single hetero-junction solar cells [8, 10] and especially nickel, *Ni*. The concept used in this report to explain observations made in $Cd_xNi_{1-x}S$ is based on the ion-to-ion model [7, 12]. In this growth condensation of Cd^{+2} and S^{-2} that results in thin film formation. The growth of $Cd_xNi_{1-x}S$ results from the incorporation of the Ni ions in the *CdS* precipitate [4, 28]. Thus a thin film photovoltaic cell is made by depositing one or more thin layers of photovoltaic material on a substrate. The substrates are immersed in an alkaline solution containing the chalcogenide source, metal ion and base. A chelating agent is added to control the release of the metal ions. Here, we report on a CBD process that promotes large area deposition [24] for efficient photovoltaic cells, sensors and lasers applications [2, 6].

MATERIAL AND METHODS

Preparation of substrates. Ordinary glass slides were used as substrates with dimensions 76.2 mm × 254 mm × 10 mm. Prior to use; they were soaked in a bath of acetone and then rinsed in dei-onized water after which they were degreased in dilute hydrochloric acid, rinsed in deionized water, dried and then stored in a desiccators ready to be used.

Growth of $Cd_xNi_{1-x}S$ thin films. The set up in Figure 1 was used. The reaction bath composed of 0.01 M $CdCl_2$ solution, 1.0 M CH_4N_2S, some drops of Concentrated NH_3 solution with varying volumes of 0.01 M $NiCl_2$ solution as tabulated in Table 1.

Table 1 – Optimized depositional Parameters for $Cd_xNi_{1-x}S$ at 0.01 M $NiCL_2$ and 0.01 M $CdCL_2$

RB	$CdCl_2$		$NiCl_2$		Value of x	Value of (1-x)
	Conc. (M)	Vol. (ml)	Conc.(M)	Vol. (ml)		
N1	0.01	10	0.01	0	1	0
N2	0.01	10	0.01	1.1	0.9	0.1
N3	0.01	10	0.01	2.5	0.8	0.2
N4	0.01	10	0.01	4.3	0.7	0.3
N5	0.01	10	0.01	6.7	0.6	0.4
N6	0.01	10	0.01	10	0.5	0.5

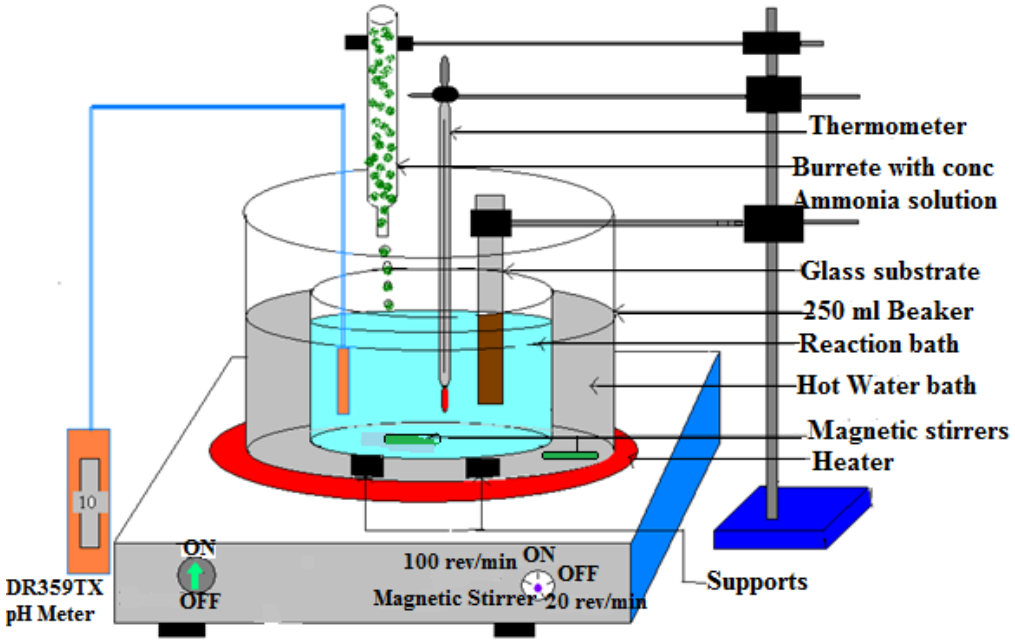

Figure 1 – Chemical bath deposition Schematic diagram

Deposition was done at 0.8 M for $NiCl_2$ and $CdCl_2$ in the order shown in Table 2 in which 10 ml $CdCl_2$ solution was put in 100 ml beaker and few drops of concentrated NH_3 solution added. Specified volumes of $NiCl_2$ solution were then added followed by accurately measured volumes of 1 M CH_4N_2S solution where the value of x varied between 1.0 and 0.5 according to the expression $Cd_xNi_{1-x}S$.

Table 2 – Optimized depositional Parameters for $Cd_xNi_{1-x}S$ at 0.8 M $NiCl_2$ and 0.8 M $CdCl_2$

RB	$CdCl_2$		$NiCl_2$		Value of x	Value of (1-x)
	Conc. (M)	Vol. (ml)	Conc. (M)	Vol. (ml)		
N7	0.8	10	0.8	0	1	0
N8	0.8	10	0.8	1.1	0.9	0.1
N9	0.8	10	0.8	2.5	0.8	0.2
N10	0.8	10	0.8	4.3	0.7	0.3
N11	0.8	10	0.8	6.7	0.6	0.4
N12	0.8	10	0.8	10	0.5	0.5

The volume of $NiCl_2$ solution was equally varied according to the formula (1):

$$x = 1 - \frac{Ni^{2+}}{Ni^{2+} + Cd^{2+}}, \quad (1)$$

where Ni^{2+} was the value of varying volume of $NiCl_2$ solution;

Cd^{2+} was the volume of $CdCl_2$ solution.

The mixture was then topped to 100 °C by adding some distilled water, placed in a warm water bath at 45 °C for 1 hour. Six samples were prepared at same deposition time. NH_3 solution was used as a complexion agent and a pH controller. Substrates were inserted at an inclined angle and after deposition; they were rinsed in distilled water; dried and kept for characterization.

Some of the thin films were annealed in a tube furnace in argon atmosphere at a temperature of 250 °C for 1 hour. The films were passivated by annealing them in a nitrogen atmosphere in a tube furnace in figure 3 for 1 hour at an average temperature of 250 °C.

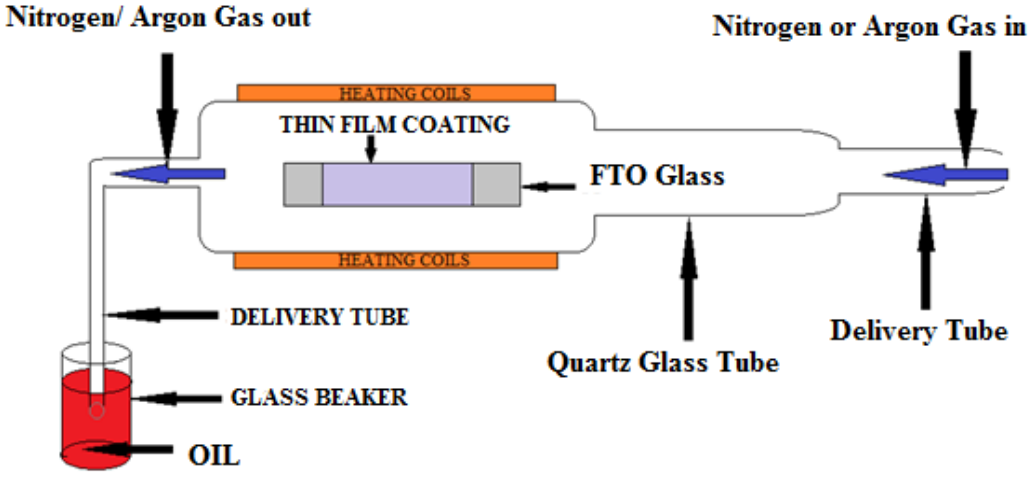

Figure 3 – Schematic diagram for a horizontal tube furnace

Optical Characterization. Transmittance measurements were measured using a computerized double beam Solid-Spec 3700 DUV Shimadzu Spectrophotometer in the spectral range from 300–1100 nm of wavelength. Scout 2.4 Software was used for simulation to obtain refractive indices, absorption coefficients, dielectric constants, real and imaginary parts and energy losses. EDX-800 HS Energy Dispersive X-rays spectrometer was used to ascertain presence of S^{2-}, Ni^{2+} and Cd^{2+} ions and their abundances (Figure 4, 5).

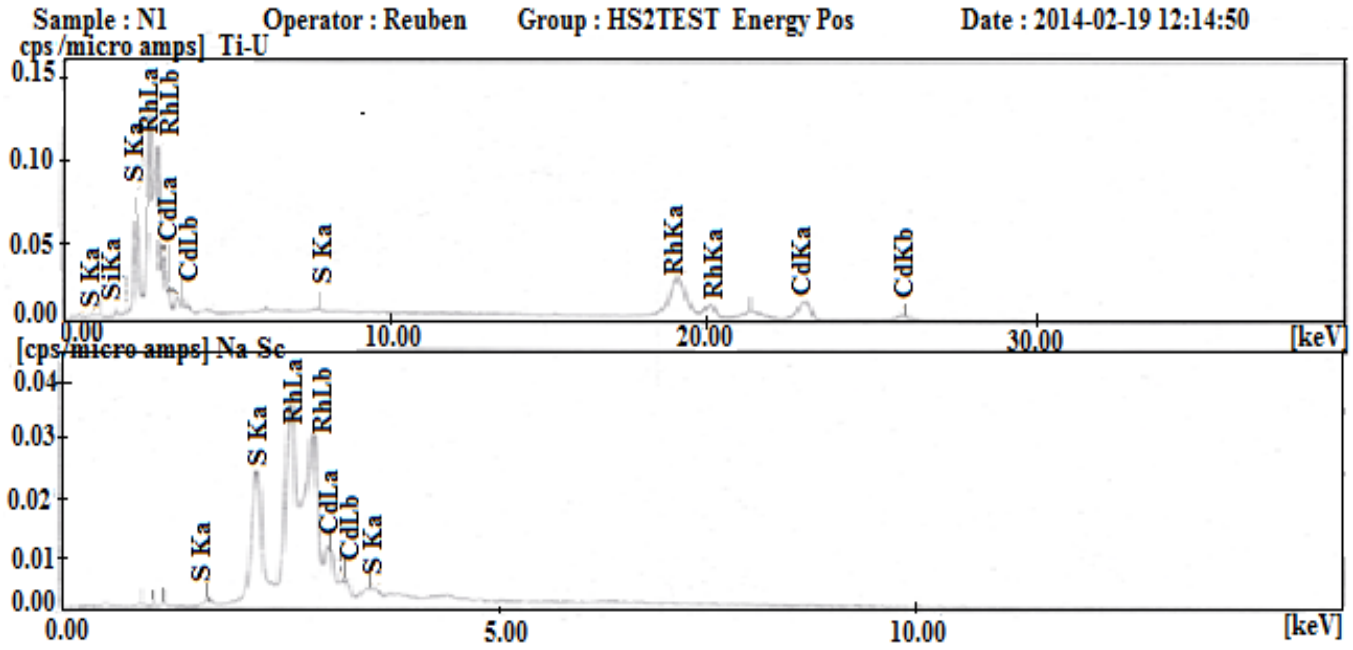

Figure 4 – XRF spectrum for as-deposited *CdS* thin film (N1) from EDX 800HS

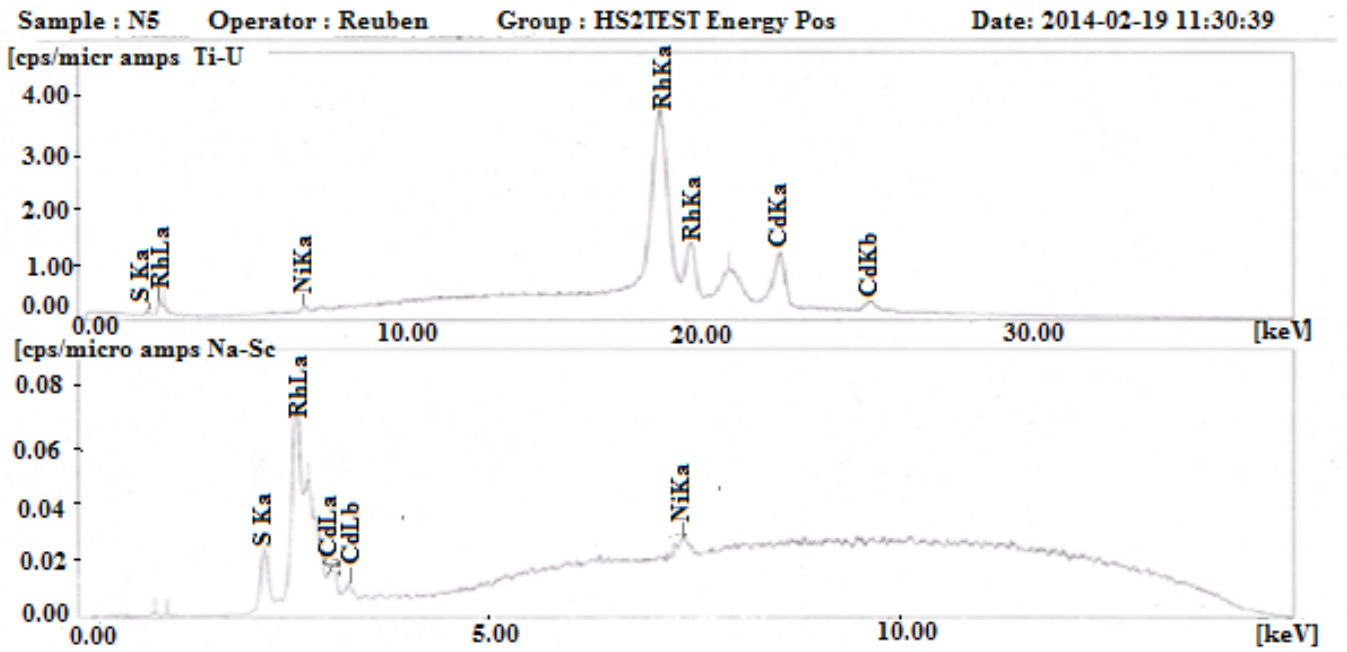

Figure 5 – XRF spectrum for as-deposited $Cd_xNi_{1-x}S$ thin film (N5) from EDX 800 HS

RESULTS AND DISCUSSION

Elemental Composition Analysis. Qualitative results in Table 3 (sample b) shows presence of *S*, *Rh*, *Ni*, *Cd* and *K* in sample N5. The sample comprised of *Cd*, *Ni* and *S* ions with *Ni* appearing in trace quantity. This implies that *Ni* acted as an impurity in $Cd_xNi_{1-x}S$ thin films. Part of the results obtained are tabulated in Table 3 (sample a) in which *S* and *Cd* were found to be the major elements in sample N1, though this include, *Si* with a trace impurity which might be due to silicon internal fluorescence peak due to the photoelectric absorption of X-rays by the silicon dead layer in the detector resulting in the emission of *Si* K-X rays from this layer into the active volume of the detector.

Table 3 – The elemental composition analysis results

Sample Analysed	Qualitative Results	Quantitative Results, %
(a) N1 – ($Cd_xNi_{1-x}S$) , x =1	S	55.223
	Cd	44.642
	Sb	0.029
	Ca	0.101
	Fe	0.005
(b)N5 – ($Cd_xNi_{1-x}S$), x = 0.6	S	21.643
	Ni	4.006
	Cd	74.345
	K	0.006

Presence of *Rh* element was as a result of the X-ray tube. Presence of *Sb*, *Ca* and *Fe* might have been caused by Spectral interference problems in EDX machine which occur at low energy (<3 keV) [25].

Optical Properties. Transmittance range was found to range between 37–44 %, 57–66 % and 83–87% in UV, VIS and NIR region respectively for $Cd_xNi_{1-x}S$ thin films deposited at 0.01 M concentration of Cd^{2+} and Ni^{2+} ions in Figure 6a while for annealed samples slightly dropped to 36–42 % in UV region, improved to 60–67 % in VIS region and remained high at 86–88 % in NIR region in Figure 6b. Highest transmittance was at 4.3 ml of nickel concentration at about 66 % and 67 % for as-grown and annealed respectively. Transmittance dropped to 12–52 %, 55–84 % and 77–86 % for as-grown films and after annealing the films (Figure 6d) respectively. The passivated films had a transmittance in the range 38–45 %, 58–68 % and 82–88% in UV, VIS and NIR region respectively (Figure 6e). The increase in transmittance spectra after annealing was attributed to enhanced crystallity and packing orderliness. This was as a result of minimal number of free carriers coupling to the electric field hence reducing the reflection and causing the transmittance to be enhanced [3]. An increase in transmittance with the volume of Cd^{2+} ions in the reaction bath was attributed to decrease in diffuse and multiple reflections caused by increase in grain size and in light-scattering effect [17, 26].

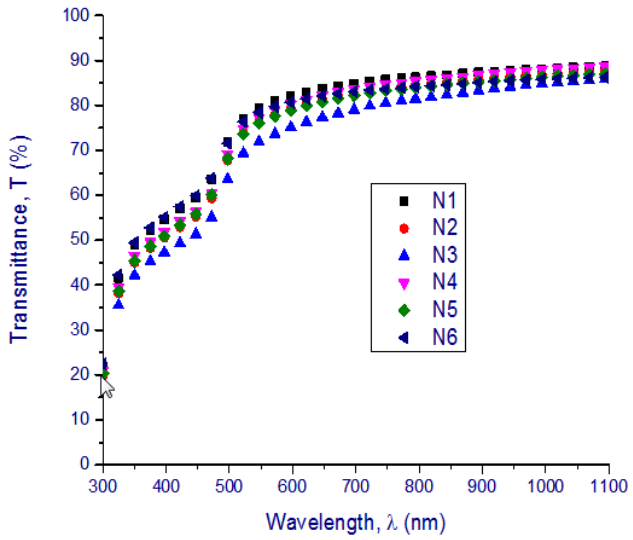

Figure 6a – Transmittance for as-deposited $Cd_xNi_{1-x}S$ films at 0.01 M of Ni^{2+} ions, %

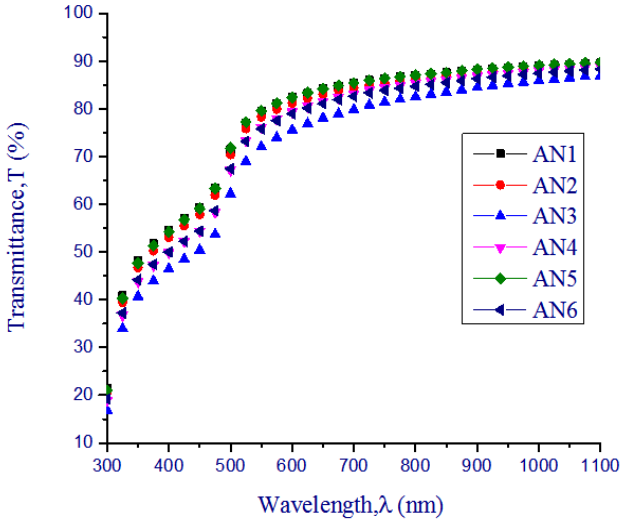

Figure 6b – Transmittance for annealed $Cd_xNi_{1-x}S$ films at 0.01 M of Ni^{2+} ions, %

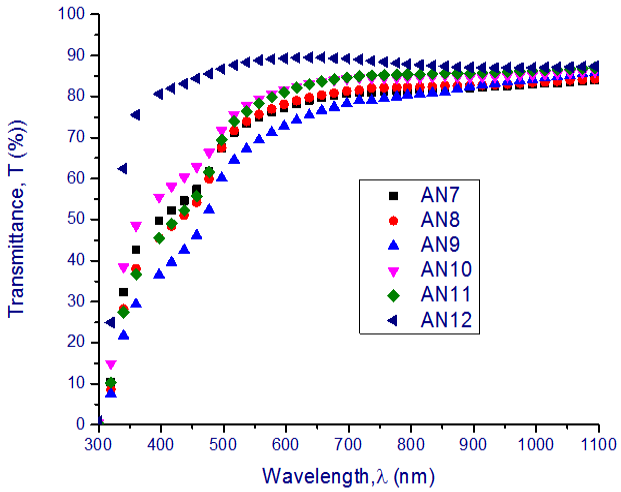

Figure 6c – Transmittance for as-deposited $Cd_xNi_{1-x}S$ films at 0.8 M of Ni^{2+} ions, %

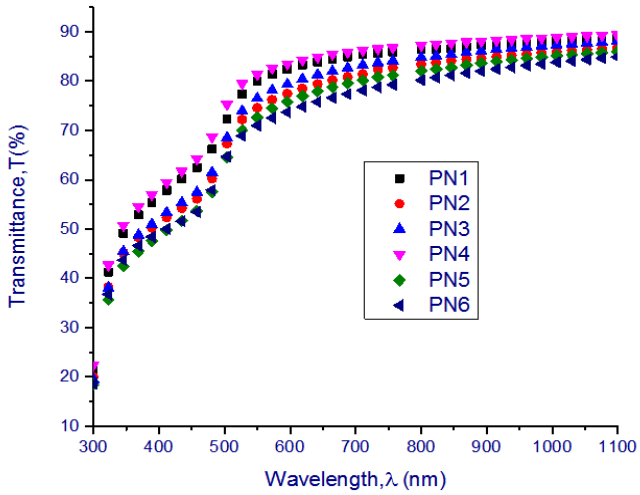

Figure 6d – Transmittance for annealed $Cd_xNi_{1-x}S$ films at 0.8 M of Ni^{2+} ions, %

In all the Figures 6, transmittance decreased as the concentration of $Cd^{2+}$and Ni^{2+} ions increased from 0.01 M to 0.8 M and this was attributed to increased free carriers coupling to the electric field hence increasing the reflection [20, 3, 16, 26]. Surface passivation had minimal influence on transmittance while an increase in transmitance at 4.3 ml of nickel ions was attributed to decrease in diffuse and multiple reflections caused by increase in grain size and in light – scattering effect [27].

Films deposited at 0.01 M concentration of ions (Figure 7a) had average reflectance range between 24–27 %, 21–30 % and 10–15 % in the UV, VIS and NIR region respectively. Annealed thin films at 0.01 M concentration (Figure 7b) had reflectance range between 21–25 %, 21–24 % and 10–13 % in the UV, VIS and NIR region respectively. Thin films deposited at 0.8 M concentration (Figure 7d) had the reflectance range decrease to between 6–14 %, 7–19 % and 7–12 % in the UV, VIS and NIR region respectively. Annealing had minimal influence on the reflectance spectra (Figure 7e).

A decrease in the reflectance was attributed to increased transmittance. With low reflectance value in the VIS-NIR region, the material is best for photovoltaic devices like solar cells as a window layer as this reduces reflective loss on the cell surface [2, 6]. Passivated thin films deposited at 0.01 M concentration of Ni^{+} ions (Figure 7c) had average reflectance range between 19–28 %, 22–28 % and 10–16% in the UV, VIS and NIR region respectively. Surface passivation had mini-

mal influence on average reflectance spectra due to optical interference which a rises as a result of difference in refractive indices of the thin films and the glass substrate used which results in multiple reflections [12, 23].

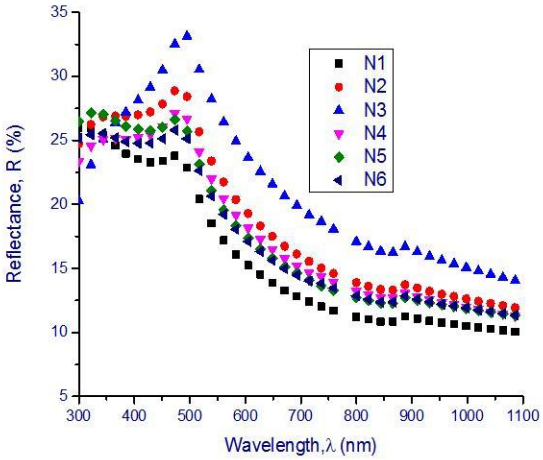

Figure 7a – Reflectance for as-deposited $Cd_xNi_{1-x}S$ thin films at 0.01 M of Ni^{2+} ions, %

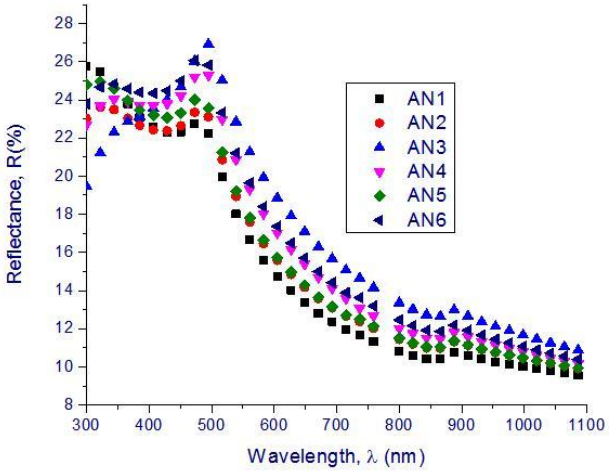

Figure 7b – Reflectance for annealed $Cd_xNi_{1-x}S$ thin at 0.01 M of Ni^{2+} ions, %

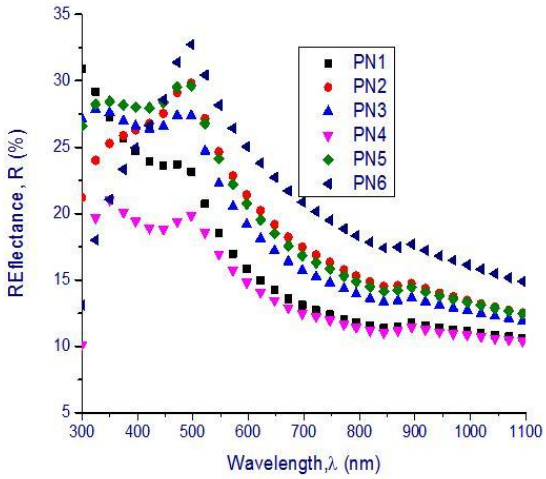

Figure 7c – Reflectance for Passivated $Cd_xNi_{1-x}S$ thin films at 0.01 M of Ni^{2+} ions, %

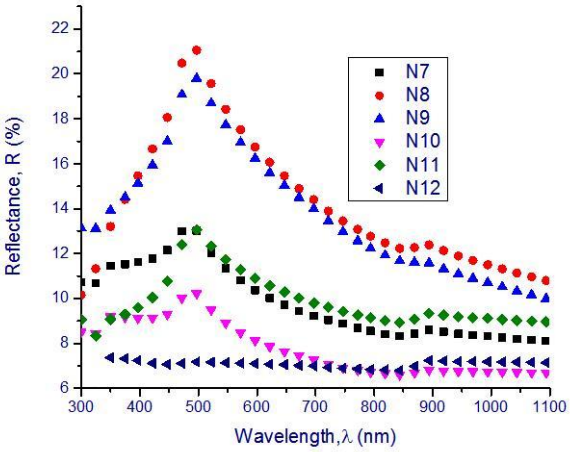

Figure 7d – Reflectance for as-deposited $Cd_xNi_{1-x}S$ thin films at 0.8 M of Ni^{2+} ions, %

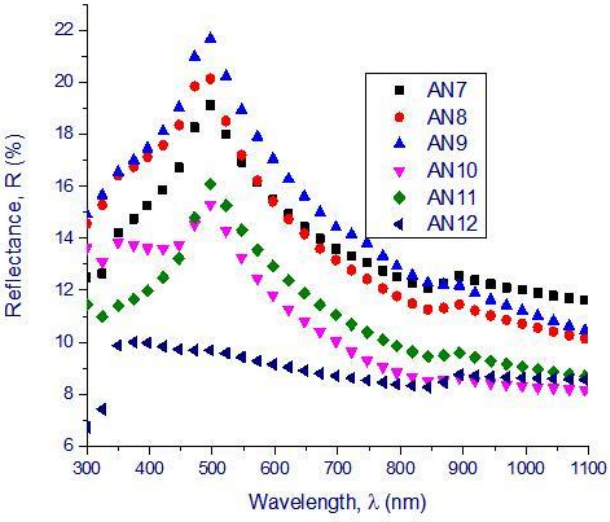

Figure 7e – Reflectance for annealed $Cd_xNi_{1-x}S$ thin films at 0.8 M of Ni^{2+} ions, %

High value of reflectance observed at 500 nm was attributed to high value of refractive index (Figure 8a–8d) with 33–42 %, 10–17 % ; 0–2 % ; 41–74 %, 9–30 % ; 9–12 % in UV, VIS and NIR region respectively [2].

The increase in the absorbance spectra with increase in the concentration of $Cd^{2+}$and Ni^{2+} ions in the reaction bath was attributed decrease in transmittance and reflectance as a result of increased photon absorption [17]. Highest value of absorption was noted at 2.5 ml doping of Ni^{2+} ions and the least value at 10 ml forming films fit for window layers in *p-n* junction solar cell [11, 25]. There was low absorption at photon energy less than 2.5 eV and 3.75 eV at 0.01 M and 0.8 M concentrations respectively. The range of the refractive index for films deposited at 0.01 M and

0.8 M ranged between 1–2 and 1–2.6 respectively. The maximum values of k and n occurred at same photon energy of 4.125 eV and these findings agree with the findings of Greenway and Harbeke [2, 7] of average magnitude for σ_0 close to 10^{12} S^{-1} and this occurs at high photon energy.

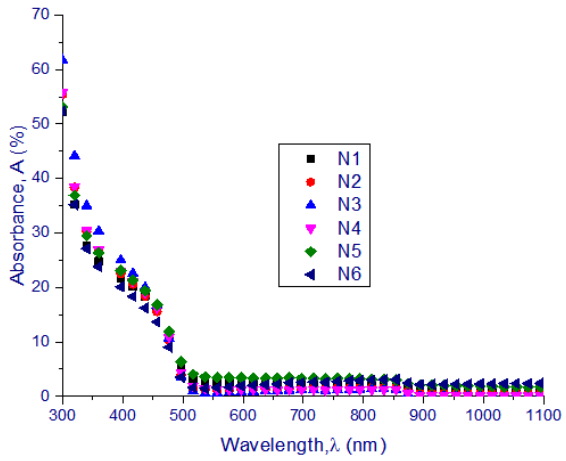

Figure 8a – Absorbance for as-deposited $Cd_xNi_{1-x}S$ thin films at 0.01 M of Ni^{2+} ions

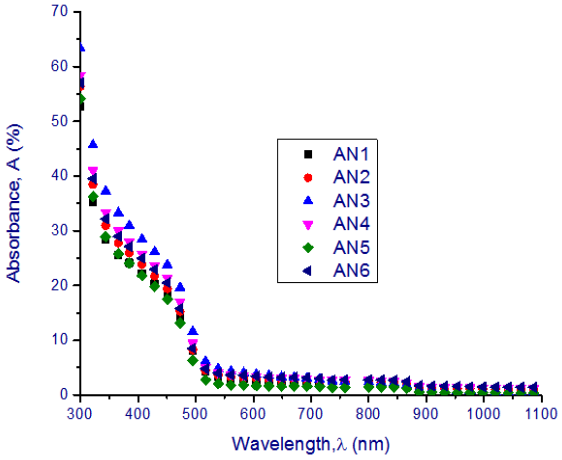

Figure 8b – Absorbance for annealed $Cd_xNi_{1-x}S$ thin films at 0.01 M of Ni^{2+} ions

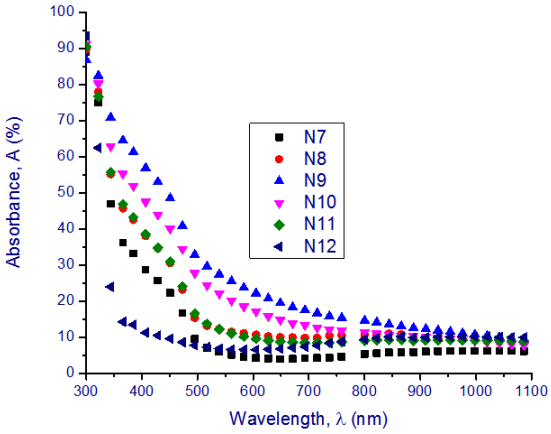

Figure 8c – Absorbance for as-deposited $Cd_xNi_{1-x}S$ thin films at 0.8 M of Ni^{2+} ions

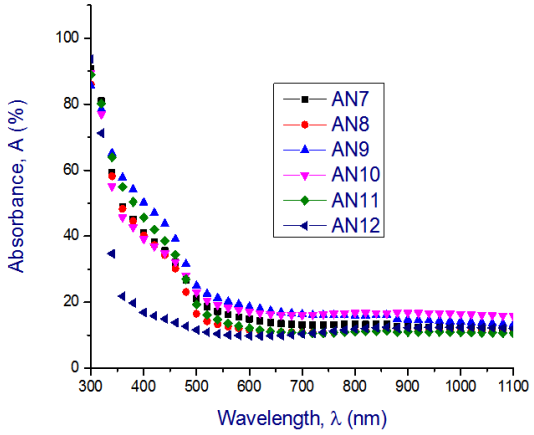

Figure 8d – Absorbance for annealed $Cd_xNi_{1-x}S$ thin films at 0.8 M of Ni^{2+} ions

The variation of α versus photon energy (Figure 8c) gave a straight line curve indicating presence of direct optical transitions [1] in which the real part indicates how the speed of light in the material can be slowed down while the imaginary part deals with the absorption of energy by a dielectric from the electric field due to dipole motion [10]. ε_r and ε_i were obtained from Scout 2.4 software by fitting the experimental transmittance data within the wavelength range 300–1100 nm. ε_r was averagely close to 2.0 from lowest to the highest photon energy values while ε_i values were below 0.5 for lower energy values and showed upward trend for energy values above 3.5 eV. The values for ε_r can be attributed to the fact that for semiconductors $k^2 << n^2$.

Band gap variation. The band gap varied between 2.55–3.17 eV (Figure 9) for as deposited films while annealing the thin films narrowed the band gap as it increased with ion concentration. An increase in the band gap attributed to the Burstein-Moss effect [17].

The decrease in the band gap due to annealing was attributed to annealing which facilitates ordered packing of crystallites of molecules reducing the intermolecular defects within the material and these causes a reduction in the band gap value [19]. High band gap values ranging between 2.56 to 3.6 eV are in good agreement with results obtained by [18] and [6]. This also increases the chance that an ejected electron will meet up with a previously created hole in the material before reaching the p-n junction [9, 15].

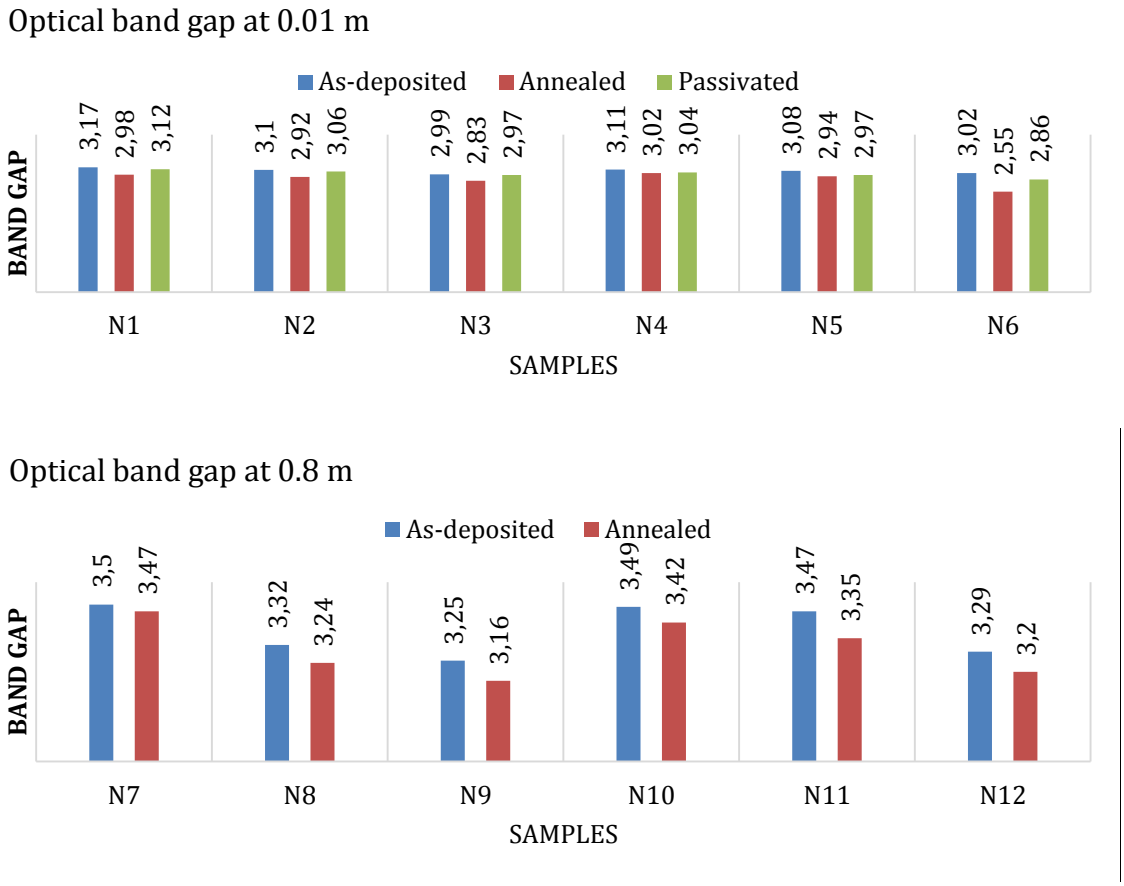

Figure 9 – Optical Band Gap for $Cd_xNi_{1-x}S$ of Ni^{2+} and Cd^{2+} ions

Effect of Passivation. Figures 6 and Figure 7c show the transmittance and reflectance spectra of as-grown passivated $Cd_xNi_{1-x}S$ thin film. Surface passivation had very little influence on transmittance and reflectance spectra since the absorbance spectra ranged from 0 % to 35 % in the VIS-NIR region for passivated thin films and 0 % to 32.5 % for as-grown and annealed thin films. Low absorption at photon energy less than 2.5 eV for passivated thin films was noted. Values obtained for these constants for as-grown, passivated and annealed thin films were within the same range. The band gap ranges were 2.85 eV–3.12 eV for passivated, 2.56 eV–3.42 eV for as-grown and 3.12 eV–3.48 eV for annealed thin films. The band gap was also least influenced by passivation.

CONCLUSION

$Cd_xNi_{1-x}S$ thin films were grown using CBD technique. The films were found to have low reflectance value in the UV-VIS-NIR regions but low transmittance values at UV region while very high transmittance at VIS-NIR regions. The average band gap has been found to be above 2.80 eV while surface passivation was found to be negligible effect on the optical properties and band gap and thus the films were well suitable for solar cell applications.

ACKNOWLEDGEMENTS

The author thank the Technical University of Mombasa, University of Nairobi, and Kenyatta University for allowing the authors to access of equipment and the technical staffs for accepting to engaged in this work. Special thanks to Mr. Muthoka and Mr. Mudimba of the University of Nairobi, Material Science laboratory and Dr. Bathsheba Kerubo Menge of the Technical University of Mombasa for the support and encouragement given to the authors during the laboratory processes.

REFERENCES

1. Amanullah, F., Al-Shammari, S., & Al-Dhafiri, A.(2005). Co-activation effect of chlorine on the physical properties of CdS thin films prepared by CBD technique for photovoltaic applications. *Physica Status Solidi (a), 202*(13), 2474–2478. doi: 10.1002/pssa.200420075
2. Asogwa, P. U., Ezugwu, S. C., Ezema, F. I., & Osuji, R. U. (2009). Influence of dip time on the optical and solid state properties of as-grown Sb_2S_3 thin films. *Chalcogenide Letters*, *6*(7), 287–292.
3. Bacaksiz, E., Aksu, S., Yilmaz, S., Parlak, M., & Altunbas, M. (2009). Structural, optical and electrical properties of Al-doped ZnO microrods prepared by spray pyrolysis. *Thin Solid Films, 518*(15), 4076–4080. doi: 10.1016/j.tsf.2009.10.141
4. Butti, K., & Perlin, J. (1981). *A golden thread: 2500 years of solar architecture and technology*. London: Boyars.
5. Chapin, D. M., Fuller, C. S., & Pearson, G. L. (1954). A New Silicon *p-n* Junction Photocell for Converting Solar Radiation into Electrical Power. *Journal of Applied Physics, 25*(5), 676-681. doi: 10.1063/1.1721711
6. Ezenwa, I. A., & Ekpunobi, A. J. (2011). Optical properties and band offsets of CdS/ZnS superlattice deposited by chemical bath. *Journal of Non-Oxide Glasses, 3*(3), 77–88.
7. Ezugwu, S. C., Ezema, F. I., & Asogwa, P. U. (2010). Synthesis and Characterization of Ternary $CuSbS_2$ Thin Films: Effect of Deposition Time. *Chalcogenide Letters*, *7*(5), 341–348.
8. Ezugwu, S. C., Ezema, F. I., Osuji, R. U., Asogwa, P. U., Ekwealor, A. B. C., & Ezekoye, B. A. (2009). Effect of deposition time on the band-gap and optical properties of chemical bath deposited CdNiS thin films. *Optoelectronics and Advanced Materials – Rapid Communications, 3*(2), 141–144.
9. Green, M. A. (2002). Third generation photovoltaics: solar cells for 2020 and beyond. *Physica E –Low-dimensional Systems and Nanostructure, 14*(1–2), 65-70. doi: 10.1016/S1386-9477(02)00361-2
10. Ilenikhena, P. A. (2008). Comparitive Studies of Improved Chemical Bath Deposited Copper Sulphide (CuS) and Zinc Sulphide (ZnS) Thin Films at 320K and Possible Applications. *African Physical Review, 2*, 59–67.
11. Isah, K. U., Hariharan, N., & Oberafo, A. (2008). Optimization of process parameters of chemical bath deposition of $Cd_{1-x}Zn_xS$ thin films. *Leonardo Journal of Sciences, 12*, 111–120.
12. Jeroh, M., & Okoli, D. (1969). Optical, Structural and Morphological Studies of Chemical Bath Deposited Antimony Sulphide Thin Film. *Global Journal of Science Frontier Research, 12*(2-A). Retrieved from https://journalofscience.org/index.php/GJSFR/article/view/369
13. Khallaf, H., Chai, G., Lupan, O., Chow, L., Heinrich, H., Park, S., & Shulte, A. (2009). In-situ boron doping of chemical-bath deposited CdS thin films. *Physica Status Solidi (a), 206*(2), 256–262. doi: 10.1002/pssa.200824290
14. Leon, M. A., & Kumar, S. (2007). Mathematical modeling and thermal performance analysis of unglazed transpired solar collectors. *Solar Energy, 81*(1), 62–75. doi: 10.1016/j.solener.2006.06.017
15. Manolache, S. A., Andronic, L., Duta, A., & Enesca, A. (2007). The influence of the deposition condition on crystal growth and on the band gap of $CuSbS_2$ thin film absorber used for Solid State Solar Cells (SSSC). *Journal of Optoelectronics and Advanced Materials, 9*(5), 1269–1272.
16. Messina, S., Nair, M. T. S., & Nair, P. K. (2007). Antimony sulfide thin films in chemically deposited thin film photovoltaic cells. *Thin Solid Films*, *515*(15), 5777–5782. doi: 10.1016/j.tsf.2006.12.155
17. Mwathe, P. M., Musembi, R., Munji, M., Odari, B., Munguti, L., Ntilakigwa, A. A., Nguu, J., Aduda, B., & Muthoka, B. (2014). Influence of surface passivation on optical properties of spray pyrolysis deposited Pd-F:SnO_2. *International Journal of Materials Science and Applications, 3*(5), 137–142.

18. Nair, P. K., Barrios-Salgado, E., Capistran, J., Ramon, M. L., Nair, M. T., & Zingaro, R. (2010). PbSe Thin Films in All-Chemically Deposited Solar Cells. *Journal of the Electrochemical Society, 157*(10), 528–537. doi: 10.1149/1.3467844

19. Nair, P. K., Ocampo, M., Fernandez, A., & Nair, M. T. (1990). Solar control characteristics of chemically deposited lead sulfide coatings. *Solar Energy Materials, 20*(3), 235–243. doi: 10.1016/0165-1633(90)90008-O

20. Odari, B. V., Musembi, R. J., Mageto, M. J., Othieno, H., Gaitho, F., Mghendi, M., & Muramba, V. (2013). Optoelectronic Properties of F-co-doped PTO Thin Films Deposited by Spray Pyrolysis. *American Journal of Materials Science, 3*(4), 91-99. doi: 10.5923/j.materials.20130304.05

21. Orori, M. C. (2012). *Electrical and optical characterization of $Cd_xZn_{1-x}S$ and PbS thin films for photovoltaic applications* (Doctoral dissertation, Kenyatta University). Retrieved from http://ir-library.ku.ac.ke/bitstream/handle/123456789/6858/Mosiori%20Cliff.pdf?sequence=1

22. Padera, F. (2013). *Measuring Absorptance (k) and Refractive Index (n) of Thin Films with the PerkinElmer Lambda 950/1050 High Performance UV-Vis/NIR Spectrometers*. Retrieved from https://ru.scribd.com/document/288823820/Thin-Films

23. Paudel, N. R., & Yan, Y. (2013). Fabrication and characterization of high-efficiency CdTe-based thin-film solar cells on commercial SnO_2:F-coated soda-lime glass substrates. *Thin Solid Film, 549*, 30–35. doi: 10.1016/j.tsf.2013.07.020

24. Reed, S. (1997). *Electron Microprobe Analysis*. Cambridge: Cambridge University Press.

25. Reynolds, J. A. (1979). An Overview of E-Beam Mask-Making. *Solid State Technology*, *22*(8), 87–94.

26. Subramanian, N. S., Santhi, B., Sundareswaran, S. & Venkatakrishnan, K. S. (2006). Studies on Spray Deposited SnO_2, Pd:SnO_2 and F:SnO_2Thin Films for Gas Sensor Applications. *Synthesis and Reactivity in Inorganic, Metal-Organic, and Nano-Metal Chemistry, 36*(1), 131–135.

27. Theiss, W. (2002). Scout Thin Film Analysis Software Handbook, Hard and Software. Retrieved from http://www.wtheiss.com/?c=2&content=applications_scout

28. Wöhrle, D., & Meissner, D. (1991). Organic solar cells. *Advanced Materials*, *3*(3), 129–138. doi: 10.1002/adma.19910030303